Supplementary Materials for

Fibrinogen-mimicking, multi-arm nanovesicles for human thrombus-specific delivery of tissue plasminogen activator and targeted thrombolytic therapy

Yu Huang, Boram Gu, Isabelle I. Salles-Crawley, Kirk A Taylor, Li Yu, Jie Ren, Xuhan Liu, Michael Emerson, Colin Longstaff, Alun D. Hughes, Simon A. Thom, Xiao Yun Xu*, Rongjun Chen*

* Corresponding authors:

E-mail addresses: rongjun.chen@imperial.ac.uk (R.C.); yun.xu@imperial.ac.uk (X.Y.X)

This PDF file includes:

Other Supplementary Materials for this manuscript include:

Videos S1 to S6

1. Supplementary experimental methods

1.1. Confocal laser scanning microscopy study

The selective binding of tPA-cRGD-PEG-NV to human activated platelets was visualized by confocal laser scanning microscopy (CLSM), with tPA fluorescently labeled by FITC. Briefly, 2 mL of human platelets (1.0×10^8 mL^{-1}) were seeded in each well of a 6-well plate, which contained a collagen-coated glass coverslip on the bottom, and activated upon incubation with 100 μL of thrombin (0.01 μM) for 10 min. Resting platelets or thrombin-activated platelets were incubated with FITC-labelled tPA-PEG-NV and tPA-cRGD-PEG-NV (equivalent tPA concentration of 0.2 mg mL^{-1}) in a shaking incubator at 37 °C, respectively. The platelets incubated with PBS buffer (pH 7.4) only were used as negative control. Then, platelets were washed twice with PBS buffer carefully and fixed with 4.0 wt% formaldehyde for 30 min. Subsequently, the platelets were visualized with a Leica SP5 MP confocal microscope.

1.2. Flow cytometry study

Flow cytometry analysis was carried out to quantitatively evaluate the selective binding of FITC-labelled tPA-cRGD-PEG-NV to human activated platelets. Briefly, 2 mL of human platelets (1.0×10^8 mL^{-1}) were placed in a tube, and activated by 100 μL of thrombin (0.01 μM) for 10 min. Then, resting platelets or thrombin-activated platelets were incubated with FITC-labelled tPA-PEG-NV and tPA-cRGD-PEG-NV (equivalent tPA concentration of 0.2 mg mL^{-1}) in a shaking incubator at 37 °C, respectively, then washed twice carefully and centrifuged at 1400 × g for 10 min, with 2 μM prostaglandin E1 as an inhibitor of platelet aggregation. The resulting samples were resuspended in a modified Tyrode's-HEPES buffer and measured by a BD Fortessa II flow cytometer and data for 1.0×10^4 gated events were collected.

1.3. Triggered tPA release at human activated platelets

The drug release study was performed to evaluate the effect of human activated platelets on the triggered tPA release behavior (*49*). Each well of a collagen-coated 96-well microplate was filled with 200 μL of human platelets at the specific concentration, which were then activated by 20 μL of thrombin (0.01 μM) under shaking. Resting platelets or thrombin-activated platelets

were incubated with tPA-PEG-NV and tPA-cRGD-PEG-NV (equivalent tPA concentration of 0.5 mg mL^{-1}) in a shaking incubator at 37 °C, respectively (*49*). The chromogenic substrate S-2251 assay was carried out quickly to measure the amount of released tPA in each well. The percentage of released tPA was determined by the following equation:

$$\%\text{Release} = \frac{A - A_{nc}}{A_{pc} - A_{nc}} \times 100 \qquad \text{(S1)}$$

where A is the absorbance of platelet samples at 405 nm treated with the tPA-loaded vesicles; A_{nc} is the absorbance of the platelet sample treated with PBS buffer (pH 7.4) only (negative control); A_{pc} is the absorbance of the platelet sample treated with the tPA-loaded vesicles lysed by Triton X-100 (positive control).

1.4. Mechanistic study of controlled tPA release

1.4.1. Human activated platelets triggered nanovesicle membrane destabilization

Calcein was encapsulated into cRGD-PEG-NV at a self-quenching concentration of 50 mM and a dequenching assay was carried out to confirm the nanovesicle membrane destabilization (*26,32,35,36*). Briefly, 200 μL of human resting or activated platelets (1.0×10^8 mL^{-1}) were placed into 1.8 mL of calcein-loaded nanovesicle solution, and the changes in calcein fluorescence at λ_{ex} = 488 nm and λ_{em} = 535 nm were monitored by a Horiba FluoroMax-4 spectrofluorometer (HORIBA, USA) under stirring. The calcein-loaded nanovesicles incubated with pH 7.4 PBS buffer only or Triton X-100 were prepared as negative and positive controls, respectively. Furthermore, human activated platelets were pre-treated with eptifibatide (100 μg mL^{-1}), an $\alpha_{IIb}\beta_3$ inhibitor which can inhibit their binding with RGD, 5 min prior to addition to the calcein-loaded nanovesicles. The percentages of calcein fluorescence intensity relative to the maximal fluorescence intensity of the positive control were calculated.

1.4.2. Membrane fusion between the nanovesicles and human activated platelets

Membrane fusion was then demonstrated to control the release of payload from cRGD-PEG-NV upon interaction with human activated platelets through a fluorescence resonance energy transfer (FRET) assay (*26,33-36*). Briefly, NBD-PE (donor) and Rhod-PE (acceptor) were coated onto the nanovesicle surface, each at 1 mol%, according to the mentioned method of nanovesicle preparation. Then, pH 7.4 PBS buffer only, 200 μL of human resting or activated platelets (1.0×10^8 mL^{-1}) were added to 1.8 mL of nanovesicle suspension under stirring. Once

the fusion between the nanovesicle membrane and the platelet membrane takes place, the density of the donor-acceptor pair will decrease, leading to the reduced FRET effect and consequently increased fluorescence intensity of the donor NBD. The NBD fluorescence at λ_{ex} = 465 nm and λ_{em} = 520 nm was monitored by a Horiba FluoroMax-4 spectrofluorometer (HORIBA, USA). Furthermore, human activated platelets were pre-treated with 100 μg mL^{-1} of eptifibatide to inhibit $\alpha_{IIb}\beta_3$ integrins 5 min prior to the addition to the nanovesicles which were incorporated with the donor NBD-PE and the acceptor Rhod-PE.

1.5. Fibrinolysis in an agar plate model

The ability of tPA-cRGD-PEG-NV to lyse human fibrin clots was evaluated by an agar plate assay (*50*). Briefly, 20 mL of agar solution (15 mg mL^{-1}) in the mixture of 50 mM Tris-HCl buffer at pH 7.2 and 25 mM $CaCl_2$ solution (3/1, v/v) was mixed with 10 mL of fibrinogen solution (10 mg mL^{-1}) in 50 mM Tris-HCl buffer (pH 7.2), followed by the addition of 10 μL thrombin (4.0 μM) under stirring for 1 min. The mixture was then transferred to a transparent plastic plate and left at 37 °C for 3 h to form a homogenous fibrin gel. Agar sample wells (~ 0.8 cm in diameter) were created in each plate and 10 μL of plasminogen solution (0.5 mg mL^{-1}) was then added into each agar well. Before adding samples into the agar wells, the nanovesicles were pre-incubated with human activated platelets to trigger tPA release. Similar to the triggered tPA release experiment described in Section 1.3 (Supplementary Materials), each well of a collagen-coated 96-well microplate was filled with 150 μL of human platelets (1.0×10^8 mL^{-1}), which were activated by 20 μL of thrombin (0.01 μM). Then, PBS, tPA-PEG-NV, tPA-cRGD-PEG-NV or free tPA (equivalent tPA concentration of 0.5 mg mL^{-1}) were co-incubated with human activated platelets in a shaking incubator at 37 °C for 2 h. The samples were centrifuged, and the resulting supernatants were added into respective agar wells and incubated at 37 °C overnight. The area of the resulting fibrin lysis zone in each agar sample well was determined to quantify the efficiency of fibrin clot lysis.

1.6. *In vitro* human platelet aggregation study

Human platelet suspensions were pre-incubated with cRGD-PEG-NV nanocarriers (lipid concentration of 10 μM) for 30 min at 37 °C. Platelets (2.5×10^8 mL^{-1}) were added to a 96-well

plate (VWR, Leicestershire, UK) containing the agonist thrombin at the specific concentration, and the plate was read at 20-s intervals for 16 min in a Power Wave X5 plate reader (Bio-TEK, Swindon, UK) (*51*). The machine was maintained at 37°C for the duration of the experiment with shaking for 7 s before each reading. Maximum aggregation at 16 min was calculated as a percentage change in absorbance, compared to baseline.

2. Supplementary experimental results

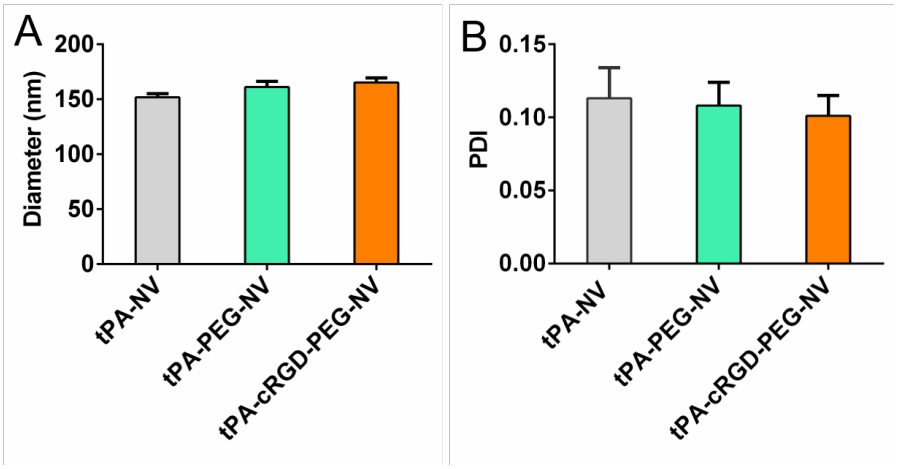

Figure S1. (A) DLS size and (B) PDI of tPA-NV, tPA-PEG-NV and tPA-cRGD-PEG-NV. Data are presented as the average ± standard deviation (n = 3).

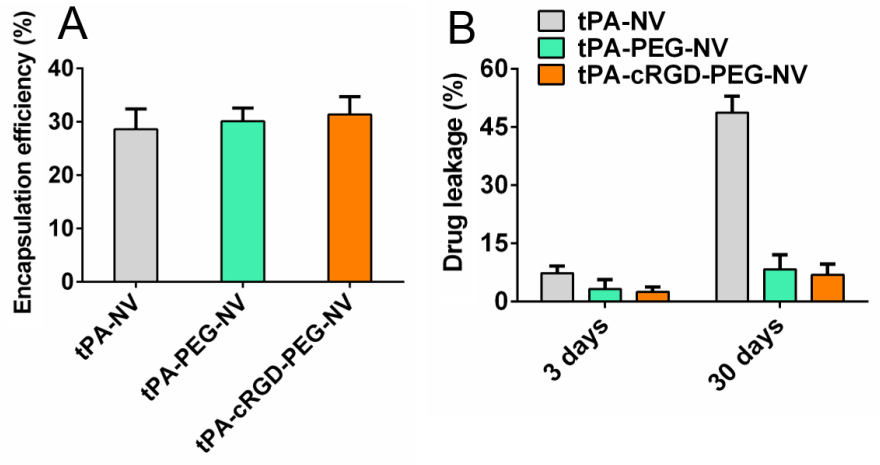

Figure S2. (A) tPA encapsulation efficiency of tPA-NV, tPA-PEG-NV and tPA-cRGD-PEG-NV. (B) Drug leakage profiles of tPA-NV, tPA-PEG-NV and tPA-cRGD-PEG-NV after storage at 4 °C for 3 and 30 days, respectively. Data are presented as the average ± standard deviation (n = 3).

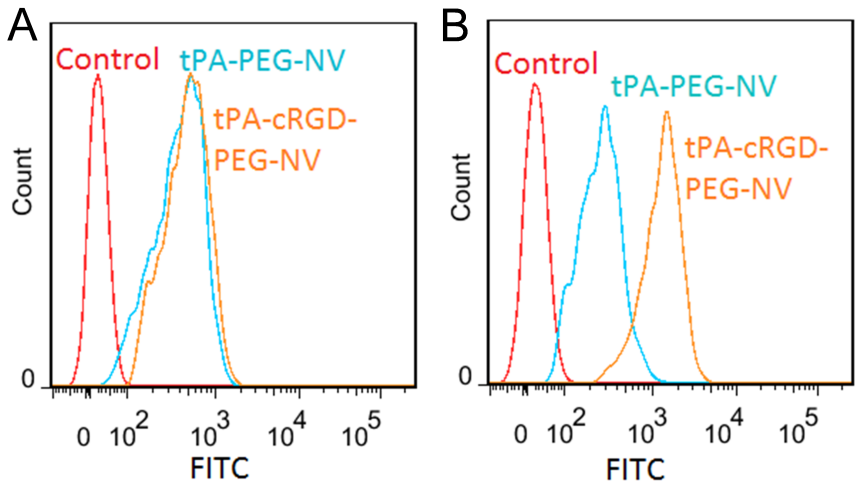

Figure S3. (A) Flow cytometry histogram profiles of human resting platelets incubated with the FITC-labelled tPA-cRGD-PEG-NV and tPA-PEG-NV, and pH 7.4 PBS buffer only (control), respectively. (B) Flow cytometry histogram profiles of human activated platelets incubated with the FITC-labelled tPA-cRGD-PEG-NV and tPA-PEG-NV, and pH 7.4 PBS buffer only (control), respectively.

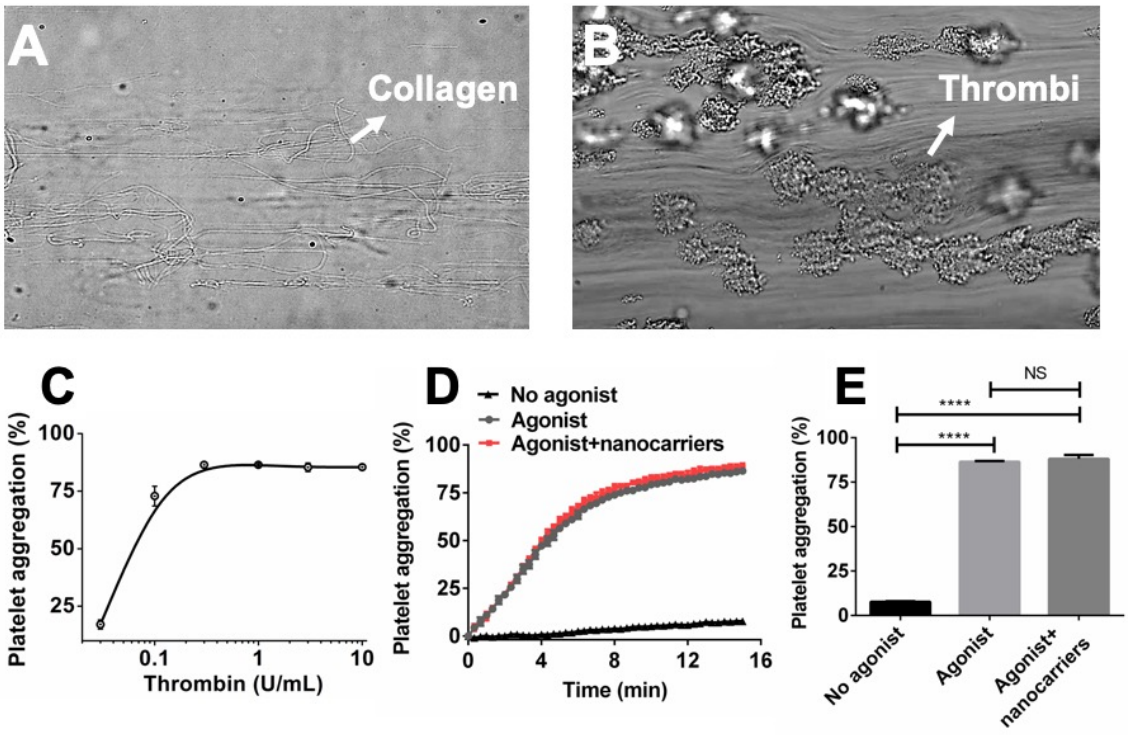

Figure S4. Citrated human blood was perfused in the collagen-coated channels at a wall shear rate of 1000 s^{-1} at room temperature to form non-occlusive thrombi. Then, the channels were

washed by perfusion with HT buffer for 2 min. Representative bright field images of (A) the channel coated with collagen and (B) human thrombi in the flow chamber of a microfluidics system. (C) Human platelet aggregation was recorded using a microplate assay following 30 min of pre-incubation with the cRGD-PEG-NV nanocarriers (lipid concentration of 10 μM) at 37 °C prior to stimulation by the agonist thrombin at concentrations of 0.03, 0.1, 0.3, 1, 3 and 10 U mL^{-1}. (D) Time-dependent human platelet aggregation was monitored and (E) maximum platelet aggregation was compared following treatment with thrombin at 1 U mL^{-1} or pre-incubation with cRGD-PEG-NV (lipid concentration of 10 μM) prior to stimulation by thrombin at 1 U mL^{-1}. The platelets without thrombin stimulation were used as the control. Data are presented as the average ± standard deviation (n =3). Statistical analysis was performed using the ANOVA (multiple comparisons) test. The quadruple asterisk symbols (****) denote $p < 0.0001$, and NS represents no significant difference between two groups.

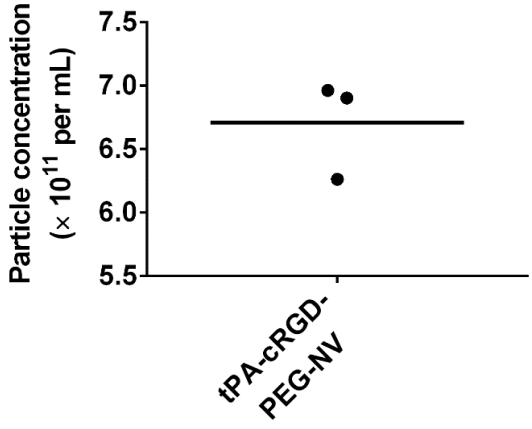

Figure S5. Particle concentration of tPA-cRGD-PEG-NV (equivalent tPA concentration of 0.314 mg mL^{-1}) in pH 7.4 PBS buffer as measured by nanoparticle tracking analysis (NTA). Data are presented as the average ± standard deviation (n = 3). 1 mL of tPA-cRGD-PEG-NV solution contained 6.70×10^{11} particles (*i.e.* 1.113×10^{-12} mol), 3.975×10^{-9} mol tPA, and 6.02×10^{16} cRGD-PEG-DSPE arms (*i.e.* 1.0×10^{-7} mol). Thus, the average molar ratio between tPA and vesicle was 3570, and the cRGD arm density was 8.985×10^4 arms per vesicle.

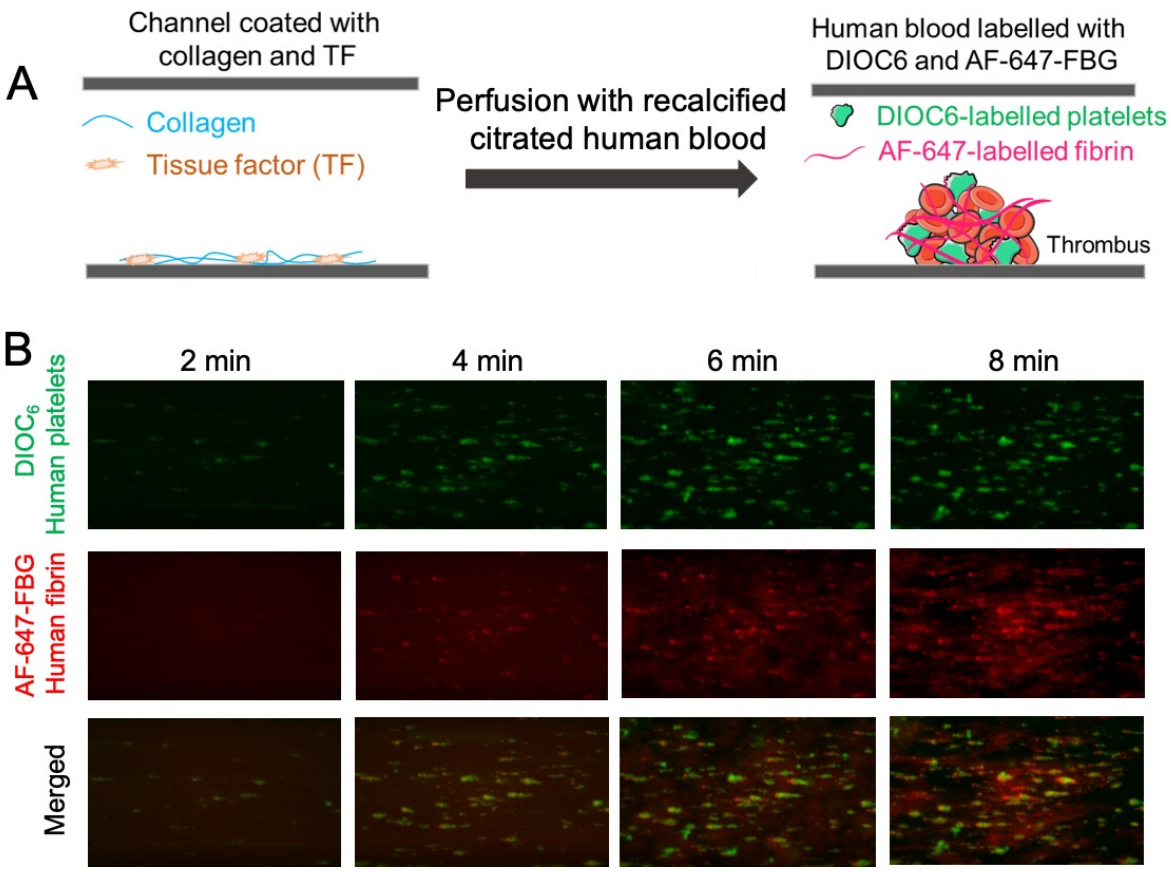

Figure S6. (A) Schematic illustration of thrombus formation and labelling in the microfluidics channel. Recalcified citrated human blood labelled with DIOC6 (green) and AF-647-FBG (red) was perfused in the collagen- and TF-coated channels for the indicated time durations at a shear rate of 1000 s^{-1} to form non-occlusive thrombi. (B) Representative fluorescence images of platelets (green) and fibrin (red) at human thrombi after perfusion with human blood for 2, 4, 6 and 8 min, respectively, in a microfluidics system.

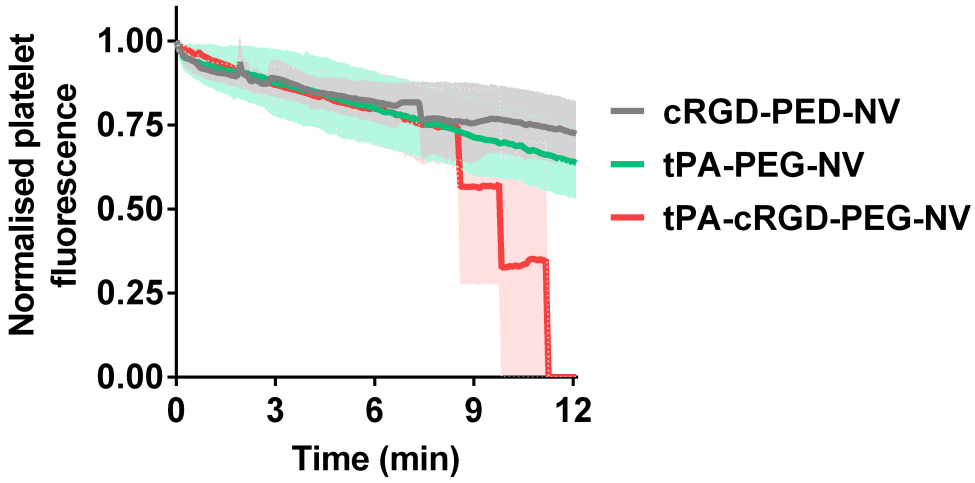

Figure S7. Real-time changes in the green fluorescence of platelets at human blood clot sites after treatment with cRGD-PEG-NV, tPA-PEG-NV and tPA-cRGD-PEG-NV, respectively, in a microfluidics system. Recalcified citrated human blood labelled with DIOC6 and AF-647-FBG was perfused in the collagen- and TF-coated channels for 8 min at a shear rate of 1000 s^{-1} to form non-occlusive thrombi. Channels were washed with HT buffer for 2 min and then the recalcified human blood containing cRGD-PEG-NV, tPA-PEG-NV and tPA-cRGD-PEG-NV, respectively, at an equivalent tPA concentration of 15 μg mL^{-1} was perfused in the thrombi-containing channels for the indicated time durations at a shear rate of 1000 s^{-1}. Data are presented as the average ± standard deviation ($n \geq 3$).

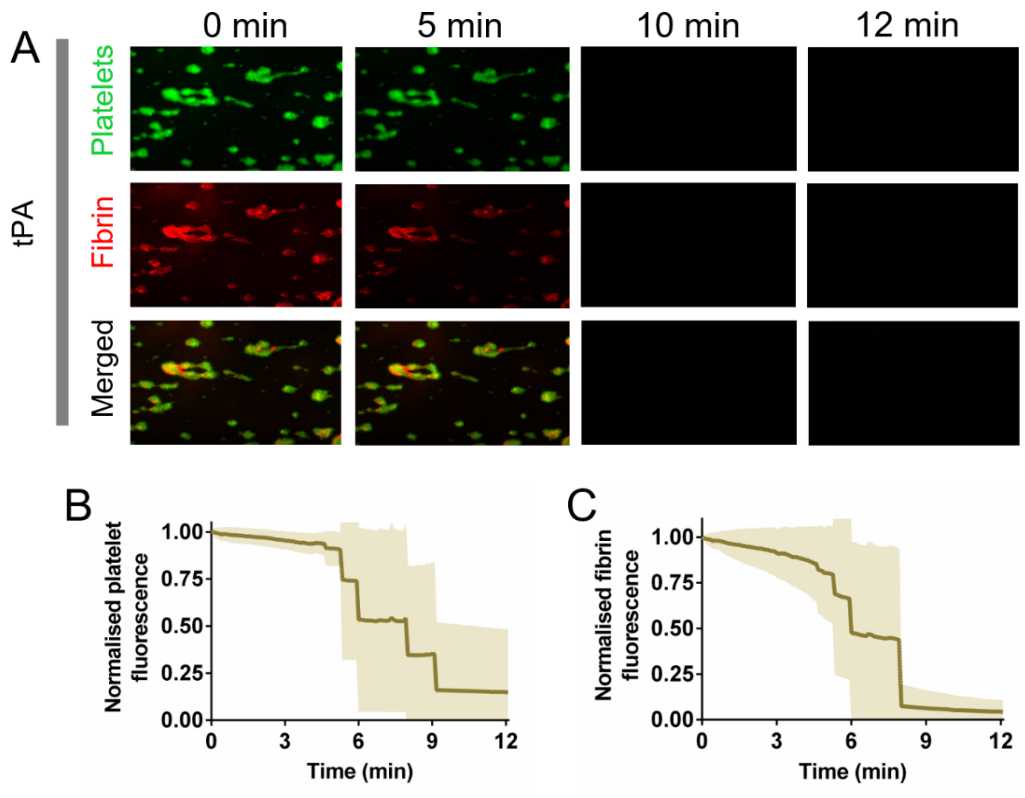

Figure S8. Recalcified citrated blood labelled with DIOC6 (green) and AF-647-FBG (red) was perfused in the collagen- and TF-coated channels for 8 min at a shear rate of 1000 s^{-1} to form non-occlusive thrombi. Channels were washed with HT buffer for 2 min, and then the recalcified blood containing free tPA (15 µg mL^{-1}) was perfused in the thrombi-containing channels for the indicated durations at a shear rate of 1000 s^{-1}. (A) Representative fluorescence images of platelets (green) and fibrin (red) at human thrombi after perfusion with free tPA at different perfusion times in a microfluidics system. (B) Real-time changes in the green fluorescence of platelets at human thrombi after perfusion with free tPA. (C) Real-time changes in the red fluorescence of fibrin at human thrombi after perfusion with free tPA. Data are presented as the average ± standard deviation ($n \geq 3$).

3. Supplementary computational modelling methods

A purpose-built computational model for thrombolysis was developed based on our previous model which was designed to simulate clot lysis during intravenous tPA therapy (*29-31*). The model was extended to incorporate the thrombolytic effect of the activated platelet-targeted ND (tPA-cRGD-PEG-NV) reported in this study. Firstly, activated platelets were included as an essential component of a thrombus in addition to a fibrin fiber network (*47*). Secondly, the transport of ND was incorporated. Thirdly, the leakage of tPA from the ND via diffusion was accounted for in the absence of activated platelets. Finally, the binding and unbinding between ND and the integrins on activated platelets and triggered release of tPA from the ND were modelled.

3.1. Reaction kinetics

Three groups of biochemical reactions take place in the targeted thrombolytic system: (i) fibrinolytic reactions in the clot phase, (ii) targeting of ND to integrins (IND) of activated platelets in thrombi and triggered release of tPA from ND, (iii) additional reactions in the plasma phase. Table S1 lists the names of species included in the model along with their abbreviations and symbols for mathematical equations. Reaction kinetics for each reaction group is followed together with their mathematical models and parameters. The model describing fibrinolytic reactions was validated in our previous work using experimental and clinical data in the literature (details on model validation can be found in Refs. 7 and 8 in the Supplementary Information).

Table S1. A list of species included in the reaction models and symbols for their concentrations (in μM).

	Name	Abbreviation	Symbol
Plasma phase or free phase	Tissue plasminogen activator	tPA	C_{tPA}
	Plasminogen	PLG	C_{PLG}
	Plasmin	PLS	C_{PLS}
	α_2-antiplasmin	AP	C_{AP}
	Plasmin-α_2-antiplasmin compound	PLS-AP	$C_{PLS\text{-}AP}$
	α_2-macroglobulin	MG	C_{MG}
	Fibrinogen	FBG	C_{FBG}
	Fibrin degradation product	FDP	-
	Plasminogen activator inhibitor-1	PAI	C_{PAI}
	Nanodrug (tPA-cRGD-PEG-NV)	ND	C_{ND}
	Nanodrug after drug release	ND_{empty}	$C_{ND,empty}$
Clot phase or fibrin-bound phase	Fibrin binding sites	F	n_{tot} (total sites), n_{free} (free sites)
	Tissue plasminogen activator	tPA^F	n_{tPA}
	Plasminogen	PLG^F	n_{PLG}
	Plasmin	PLS^F	n_{PLS}
	Degraded fibrin site with plasmin	$\not{P}LS^F$	-
	Degraded fibrin site	$\tilde{F}$	n_{deg}
Platelet associated	Activated platelets	PLT	C_{PLT}
	$\alpha_{IIb}\beta_3$ integrins	INT	$C_{INT,tot}$ (total sites), $C_{INT,free}$ (free sites)
	Integrin-bound ND	ND^{INT}	$C_{INT\text{-}ND}$
	Integrin-bound empty ND	ND_{empty}^{INT}	$C_{INT\text{-}ND,empty}$

3.1.1. Fibrinolytic reactions for clot dissolution

$$\mathrm{tPA} + \mathrm{F} \underset{k_{d,tPA}}{\overset{k_{a,tPA}}{\rightleftharpoons}} \mathrm{tPA^F}, \quad r_{tPA} = k_{a,tPA} C_{tPA} n_{free} - k_{d,tPA} n_{tPA} \tag{S2}$$

$$\mathrm{PLG} + \mathrm{F} \underset{k_{d,PLG}}{\overset{k_{a,PLG}}{\rightleftharpoons}} \mathrm{PLG^F}, \quad r_{PLG} = k_{a,PLG} C_{PLG} n_{free} - k_{d,PLG} n_{PLG} \tag{S3}$$

$$\mathrm{PLS} + \mathrm{F} \underset{k_{d,PLS}}{\overset{k_{a,PLS}}{\rightleftharpoons}} \mathrm{PLS^F}, \quad r_{PLS} = k_{a,PLS} C_{PLS} n_{free} - k_{d,PLS} n_{PLS} \tag{S4}$$

$$\mathrm{PLG^F} \underset{KM,k_{cat}}{\overset{tPA^F}{\rightleftarrows}} \mathrm{PLS^F},\ r_{PLS,MM} = \frac{k_{cat} n_{PLG} n_{tPA}}{K_M\left(1-\varepsilon_{clot}\right)+n_{PLG}} \tag{S5}$$

$$\mathrm{PLS^F} \xrightarrow{k_{deg}} \cancel{\mathrm{PLS}}^{\mathrm{F}},\ r_{dgr} = k_{dgr}\gamma n_{PLS} \tag{S6}$$

$$\cancel{\mathrm{PLS}}^{\mathrm{F}} \xrightarrow{k_{d,PLS}} \mathrm{PLS} + \tilde{\mathrm{F}},\ r_{PLS,return} = k_{d,PLS} n_{\mathrm{deg}} \tag{S7}$$

3.1.2. Targeting and triggered release

$$\mathrm{ND} + \mathrm{INT} \underset{k_{d,ND}}{\overset{k_{a,ND}}{\rightleftarrows}} \mathrm{ND^{INT}},\ r_{ND} = k_{a,ND} C_{ND} C_{INT,free} - k_{d,ND} C_{INT-ND} \tag{S8}$$

$$\mathrm{ND^{INT}} \xrightarrow{k_{rel}} \nu_{rel}\,\mathrm{tPA^F\ (or\ tPA\ for\ plasma\ PLT)} + \mathrm{ND_{empty}}^{\mathrm{INT}},\ r_{rel} = k_{rel} C_{ND-INT} \tag{S9}$$

$$\mathrm{ND_{empty}} + \mathrm{INT} \underset{k_{d,ND}}{\overset{k_{a,ND}}{\rightleftarrows}} \mathrm{ND_{empty}}^{\mathrm{INT}},\ r_{ND,empty} = k_{a,ND} C_{ND,empty} C_{INT,free} - k_{d,ND} C_{INT-ND,empty} \tag{S10}$$

$$\mathrm{ND} \xleftarrow{K_{leak}} \nu_{rel}\,\mathrm{tPA} + \mathrm{ND_{empty}},\ r_{leak} = K_{leak}\left(\nu_{rel} C_{ND} - C_{tPA}\right) \tag{S11}$$

3.1.3. Plasma reactions

$$\mathrm{PLG} \underset{K_{M,PLG},k_{cat,PLG}}{\overset{tPA}{\rightleftarrows}} \mathrm{PLS},\ r_{tPA-PLG} = \frac{k_{cat,PLG} C_{tPA} C_{PLG}}{K_{M,PLG} + C_{PLG}} \tag{S12}$$

$$\mathrm{FBG} \underset{K_{M,FBG},k_{cat,FBG}}{\overset{PLS}{\rightleftarrows}} \mathrm{FDP},\ r_{PLS-FBG} = \frac{k_{cat,FBG} C_{PLS} C_{FBG}}{K_{M,FBG} + C_{FBG}} \tag{S13}$$

$$\mathrm{PLS} + \mathrm{AP} \underset{k_{AP,r}}{\overset{k_{AP,f}}{\rightleftarrows}} \mathrm{PLS\text{-}AP} \xrightarrow{k_{cat,AP}} \mathrm{inactive},\ r_{AP,1} = k_{AP,f} C_{PLS} C_{AP} - k_{AP,r} C_{PLS-AP},\quad r_{AP,2} = k_{cat,AP} C_{PLS-AP} \tag{S14}$$

$$\mathrm{PLS} + \mathrm{MG} \xrightarrow{k_{MG}} \mathrm{PLS\text{-}MG},\ r_{MG} = k_{MG} C_{PLS} C_{MG} \tag{S15}$$

$$\mathrm{tPA} + \mathrm{PAI} \xrightarrow{k_{PAI}} \mathrm{tPA\text{-}PAI},\ r_{PAI} = k_{PAI} C_{tPA} C_{PAI} \tag{S16}$$

The concentration of free INT sites can be calculated as follows:

$$C_{INT,free} = C_{INT,tot} - \left(C_{INT-ND} + C_{INT-ND,dam}\right) \tag{S17}$$

$$C_{INT,tot} = N_{INT} C_{PLT} \tag{S18}$$

Likewise, the concentration of free F sites is:

$$n_{free} = n_{tot} - (n_{tPA} + n_{PLG} + n_{PLS}) \quad \text{(S19)}$$

3.2. Properties of blood clots composed of fibrin fiber network and activated platelets

3.2.1. Estimation of the initial binding sites, F and INT

The Materials and Methods Section "Computational modelling" in the manuscript gave a brief description of how the initial properties of thrombus components, i.e. fibrin fiber network and activated platelets, can be estimated. Detailed model equations are included herein. Once the initial volume fraction of fibrin fibers $\Phi_{f,0}$ and activated platelets $\Phi_{p,0}$ are determined, the concentrations of total F and INT, $n_{tot,0}$ and $C_{INT,tot,0}$ can be calculated.

$$\Phi_{tot,0} = \Phi_{f,0} + \Phi_{p,0} \quad \text{(S20)}$$

$$\varepsilon_{tot,0} = 1 - \Phi_{tot,0} \quad \text{(S21)}$$

$$C_{PLT,0} = \frac{P_{max}\Phi_{p,0}}{N_{AV}} \quad \text{(S22)}$$

$$n_{tot,0} = \frac{2 \times CS_V \times BS_{CS}}{N_{AV}},$$
$$\text{where } BS_{CS} = \sum_{i=1}^{N_{CS+1}} \frac{\pi}{sin^{-1}\frac{d\theta}{2idr}}, CS_V = \frac{LtVt}{0.5L_M}, LtVt = \frac{\Phi_{f,0}}{\pi R_f^2} \text{ and } N_{CS} = \frac{R_f}{dr} \quad \text{(S23)}$$

Using Eqs (S18) and (S22), $C_{INT,tot,0}$ can be obtained. Further details on the derivation of Eq (S23) can be found in our previous study (*29*).

3.2.2. Calculation of thrombus properties

The total thrombus resistance to blood flow can be expressed as the sum of resistances imposed by its constituents, i.e. the fibrin fiber network and activated platelets (*52*). This is an important variable as it represents the inverse of thrombus permeability and is added to the momentum transport equation later for flow simulation.

$$R_{clot,tot} = R_{clot,f} + R_{clot,p} \quad \text{(S24)}$$

$$R_{clot,f} = \begin{cases} \dfrac{16\Phi_f^{1.5}\left(1+56\Phi_f^3\right)}{R_f^2}, & E_L \le E_{L,crit} \\ 0, & E_L > E_{L,crit} \end{cases} \tag{S25}$$

$$R_{clot,p} = \begin{cases} \dfrac{150\Phi_p^2}{S_p^2 D_p^2\left(1-\Phi_p\right)^3}, & E_L \le E_{L,crit} \\ 0, & E_L > E_{L,crit} \end{cases} \tag{S26}$$

where R_{clot} is the thrombus resistance and the subscripts *tot*, *f* and *p* denote total, fibrin fibers and platelets, respectively. E_L is the extent of fibrinolysis, R_f the radius of fibrin fibers, D_p the platelet diameter and S_p the sphericity. Therefore, the permeability contributed by each part is calculated as:

$$k_{clot,i} = \frac{1}{R_{clot,i}} \text{ where } i = p, f, tot \tag{S27}$$

As fibrinolysis progresses, the volume fraction of each component varies. The volume fraction of fibrin fiber network is updated based on the extent of lysis E_L:

$$E_L = 1 - \frac{n_{tot}}{n_{tot,0}} \tag{S28}$$

$$\Phi_f = \Phi_{f,0}\left(1-E_L\right) \tag{S29}$$

On the other hand, the volume fraction of activated platelets is based on the relative amount of platelets E_{PLT} in the blood clot, as platelet contents might not be proportional to the extent of fibrinolysis due to its larger size.

$$E_{PLT} = \frac{C_{PLT}}{C_{PLT,0}} \tag{S30}$$

$$\Phi_p = \Phi_{p,0} E_{PLT} \tag{S31}$$

3.3. Descriptions of reaction model parameters and their values

A list of model parameters and their values used in the simulations presented in this work are given in Table S2. The kinetics parameters associated with our newly developed ND were derived from our experimental results, shown in Figure 5 in the manuscript. Due to the limited number of experimental data sets, multiple sets of three parameters were obtained from

parameter estimation. A set of parameters whose values were the closest match to the counterpart parameters of tPA, $k_{a,tPA}$ and $k_{d,tPA}$ was selected. Other reaction kinetics parameters were kept the same as in our previous work (*29,30*), where justification for the chosen values and validation against experimental data can be found, unless otherwise stated.

Table S2. Model parameters and their values

Symbol	Description	Value	Unit	Source
$k_{a,tPA}$	Adsorption coefficient for tPA	0.01	$\mu M^{-1}\ s^{-1}$	Ref. 29
$k_{d,tPA}$	Desorption coefficient for tPA	0.0058	s^{-1}	Ref. 29
$k_{a,PLG}$	Adsorption coefficient for PLG	0.1	$\mu M^{-1}\ s^{-1}$	Ref. 29
$k_{d,PLG}$	Desorption coefficient for PLG	3.8	s^{-1}	Ref. 29
$k_{a,PLS}$	Adsorption coefficient for PLS	0.1	$\mu M^{-1}\ s^{-1}$	Ref. 29
$k_{d,PLS}$	Desorption coefficient for PLS	0.05	s^{-1}	Ref. 29
K_M	Michaelis constant for PLG conversion in the bound phase	0.1	μM	Ref. 29
k_{cat}	Michaelis reaction rate coefficient for PLG conversion in the bound phase	0.3	s^{-1}	Ref. 29
k_{deg}	Lysis coefficient	2.178	s^{-1}	Ref. 29
$1/\gamma$	Cuts needed for PLS to cut 1 fibrin unit	10	-	Ref. 29
$k_{a,ND}$	Adsorption coefficient for ND	2.6224×10^{-2}	$\mu M^{-1}\ s^{-1}$	From our experiment
$k_{d,ND}$	Desorption coefficient for ND	7.5159×10^{-3}	s^{-1}	From our experiment
k_{rel}	Triggered release rate constant	0.10975	s^{-1}	From our experiment
K_{leak}	Leakage rate constant	2.946×10^{-9}	s^{-1}	From our experiment
$K_{M,PLG}$	Michaelis constant for PLG	28.03	μM	Ref. 30

	conversion in the free phase			
$k_{cat,PLG}$	Michaelis reaction rate coefficient for PLG conversion in the free phase	0.3	s^{-1}	Ref. 30
$K_{M,FBG}$	Michaelis constant for FBG conversion in the free phase	55	μM	Ref. 30
$k_{cat,FBG}$	Michaelis reaction rate coefficient for FBG conversion in the free phase	250	s^{-1}	Ref. 30
$k_{AP,f}$	Forward reaction constant for AP and PLS	10	$\mu M^{-1}\ s^{-1}$	Ref. 30
$k_{AP,r}$	Reverse reaction constant for AP and PLS	0.0021	s^{-1}	Ref. 30
$k_{cat,AP}$	Inactivation rate constant by AP	0.004	s^{-1}	Ref. 30
k_{MG}	Reaction constant for MG and PLS	0.35	$\mu M^{-1}\ s^{-1}$	Ref. 30
k_{PAI}	Reaction constant for tPA and PAI	37	$\mu M^{-1}\ s^{-1}$	Ref. 30
ν_{rel}	Stochiometric coefficient for tPA and ND reaction	3,570	-	Figure S5
N_{INT}	Number of integrins expressed upon activation of platelets	80,000	numbers	Ref. 16
P_{max}	Max. number of platelets per unit volume	6.67×10^{13}	numbers	Ref. 48
R_f	Fibrin fibre radius	50	nm	Ref. 44
L_M	Length of fibrin monomer	45	nm	Ref. 44
dr	Protofibril inter-spacing in r-direction	10	nm	Ref. 29
$d\theta$	Protofibril inter-spacing in θ-direction	10	nm	Ref. 29
S_p	Sphericity of platelets	1	-	Ref. 52
D_p	Platelet diameter	2	μm	Ref. 52
$E_{L,crit}$	Critical extent of lysis	0.95	-	Ref. 29

3.4. Model equations for flow and species transport

The fundamental equations include those governing the fluid flow and species transport accounting for convection, diffusion and reaction. First, model equations applicable to the continuous system are presented. Under flow conditions, the modified Navier-Stokes equations were used to describe blood flow in the presence of thrombi, assuming incompressible and Newtonian flow.

$$\nabla \cdot \mathbf{u} = 0 \tag{S32}$$

$$\rho\left(\frac{\partial \mathbf{u}}{\partial t} + \mathbf{u} \cdot \nabla \mathbf{u}\right) = -\nabla p + \mu \nabla^2 \mathbf{u} - \frac{\mu}{k_{clot,tot}} \mathbf{u} \tag{S33}$$

where $\mathbf{u}$ is the velocity, p the pressure, ρ the density, μ the viscosity and $k_{clot,tot}$ the blood clot permeability.

For the species transport, the convection-diffusion-reaction equations were used for each component present in the free phase.

$$\frac{\partial C_j}{\partial t} = -\nabla \cdot \left(\mathbf{u} C_j\right) + D_j \nabla^2 C_j + r_{tot,j}, \tag{S34}$$
$$\text{for } j = \text{tPA, PLG, PLS, ND, ND}_{empty}\text{, AP, PLS-AP, FBG, MG and PAI}$$

where C_j is the concentration of component j, D_j the diffusivity of component j and $r_{tot,j}$ the source term of the total reactional contributions. The source term for each component consists of the rates of reactions where each component is involved. For example, the source term $r_{tot,ND}$ for C_{ND} is:

$$r_{tot,ND} = -r_{ND} - r_{leak} \tag{S35}$$

For the transport of activated platelets, a new term, a mobility function, M, was introduced to simulate limited movement of activated platelets trapped within the fibrin fiber network that was not sufficiently dissolved to free up the activated platelets.

$$\frac{\partial C_{PLT}}{\partial t} = -M \cdot \nabla \cdot \left(\mathbf{u} C_{PLT}\right) + M \cdot D_{PLT} \nabla^2 C_{PLT} \tag{S36}$$

where M is the mobility function. We used a simple form for M

$$M = \begin{cases} 1, \text{ if } E_L > E_{L,crit} \\ 0, \text{ if } E_L \le E_{L,crit} \end{cases} \tag{S37}$$

For the fibrin- or integrin-bound phase, the convective ($\mathbf{u}$) and diffusive terms (D_j) were removed.

$$\frac{\partial C_k}{\partial t} = r_{tot,k}, \text{ for } k = \text{INT-ND}, \text{INT-ND}_{\text{empty}} \quad \text{(S38)}$$

$$\frac{\partial n_l}{\partial t} = r_{tot,l}, \text{ for } l = \text{tPA, PLG, PLS and deg} \quad \text{(S39)}$$

n_{tot} is determined by the degradation of binding sites by bound PLS.

$$\frac{\partial n_{tot}}{\partial t} = -r_{dgr} \quad \text{(S40)}$$

To simulate the experiments under static conditions, the convective (**u**) and diffusive terms (D_j) were removed, and the system was assumed to be perfectly mixed.

4. Supplementary computational simulation details

4.1. Static conditions

For simulations of the static experiments, the initial concentrations of the species are listed in Table S3, or calculated based on Table S3 and Eqs (S20)-(S23). A set of ordinary differential equations were solved numerically via ode15s in MATLAB 2019b. A time step of 1 sec was used.

Table S3. Initial conditions for simulations of the static experiments

	Selected value	**Typical value in the plasma [source]**
Initial volume fraction of fibrin fiber, $\Phi_{f,0}$	0.025	Blood clot porosity > 0.75 [Ref. 44]
Initial volume fraction of platelets, $\Phi_{p,0}$	0.1	Blood clot porosity > 0.75 [Ref.44]
Initial concentration of tPA (or ND)	2.152 μM (or $2.152/\nu_{rel}$)	Our experiment
Initial concentration of PLG	2.2 μM	2.2 μM [Ref. 44]
Initial concentration of PLS	0 μM	0 μM [Ref. 44]
Initial concentration of FBG	8 μM	8 μM [Ref. 44]
Initial concentration of AP	0.5 μM	1 μM [Ref. 44]
Initial concentration of MG	1.5 μM	3 μM [Ref. 44]
Initial concentration of PAI	5.23e-04 μM	5.23×10^{-4} μM [Ref. 45]

4.2. Flow simulation

Computational mesh for the thrombi-containing rectangular channel shown in Figure 1D of the Manuscript was generated using ICEM CFD 15.0. The mesh consisted of 384,274 hexahedral elements, which was sufficiently fine to ensure mesh-independent solution. Boundary and initial conditions and model parameters are shown in Tables S4 and S5, respectively. Initial concentrations are the same as the typical plasma concentrations listed in Table S3, unless otherwise stated. Model equations were coded in the C++ programming language and implemented in OpenFOAM 4.0, an open source computational fluid dynamics (CFD) code. The PIMPLE algorithm was adopted for pressure-velocity coupling. A tolerance of 10^{-5} and 5×10^{-5} for velocity and pressure were chosen to ensure convergence and sufficient accuracy within each time step of 0.005 s. Results were saved every 1 second throughout the entire simulation time or 0.05 second for a short time period where clot dissolution is expected.

Table S4. Boundary conditions

Location	Velocity	Pressure	Concentration
Inlet	Average velocity, u_0 = 0.0167 m s^{-1}	Zero gradient	Constant for each component, $C_{tPA,in}$ = 0.03 μM, $C_{ND,in}$ = 8.4×10^{-6} μM (equivalent to 0.03 μM of tPA). Other parameters are the same as those in Table S3.
Outlet	Zero gradient	Zero pressure	Zero gradient
Walls	No slip	Zero gradient	Zero gradient

Table S5. Initial conditions and other model parameters

	Value [unit]
Initial volume fraction of fibrin fibre, $\Phi_{f,0}$	0.001 [-]
Initial volume fraction of platelets, $\Phi_{p,0}$	0.01 or 0.05 [-]
Initial concentration of tPA	0.05×10^{-3} [μM]
Fibrin radius, R_f	100 [nm]
Diffusivity of all the fibrinolytic proteins, D_{prt}	5×10^{-11} [m^2 s^{-1}]
Diffusivity of platelets, D_{PLT}	2.5×10^{-12} [m^2 s^{-1}]
Diffusivity of ND, D_{ND}	2.5×10^{-11} [m^2 s^{-1}]
Blood density, ρ	1,060 [kg m^{-3}]
Blood viscosity, μ	3.5×10^{-3} [Pa s]

5. Supplementary computational simulation results

5.1. Comparisons between computational and experimental results

For the halo blood clot lysis experiment, the initial properties of the clot and the concentrations of all fibrinolytic proteins should ideally be measured and used in our computational simulations. However, it is challenging to quantify the internal structure of the formed blood clot, e.g., the volume fractions of fibrin fibers and activated platelets. Furthermore, some plasma proteins could become inactive during blood clot incubation (*39*), making it difficult to employ a typical level of fibrinolytic proteins in the circulating plasma. These limitations should be borne in mind when making comparisons between the computational and experimental results. The initial conditions of the halo shaped human blood clot were estimated by starting from a typical set of values (refer to Table S3 for the selected initial conditions and their typical values) and then adjusting these values to fit the experimental data for blood clot lysis with tPA (shown in Figure 5F in the Manuscript). The same initial conditions were assumed for thrombolysis with the ND. The tPA dose was set to be identical to the experimental conditions stated in the Halo assay. As can be seen in Figure S9, at the given condition, the model predicted the extent of blood clot lysis reasonably well for the case of free tPA. However, the predicted thrombolysis by the ND (the orange dashed line in Figure S9) deviated significantly from the experimental data. In fact, the simulation results showed much smaller differences in the extent of clot lysis between free tPA and the ND than experimental measurements. Possible reasons for the discrepancy between the model prediction and experiment are explained in the Results and Discussion Section “Computational simulation of tPA release and blood clot lysis under static conditions” in the manuscript.

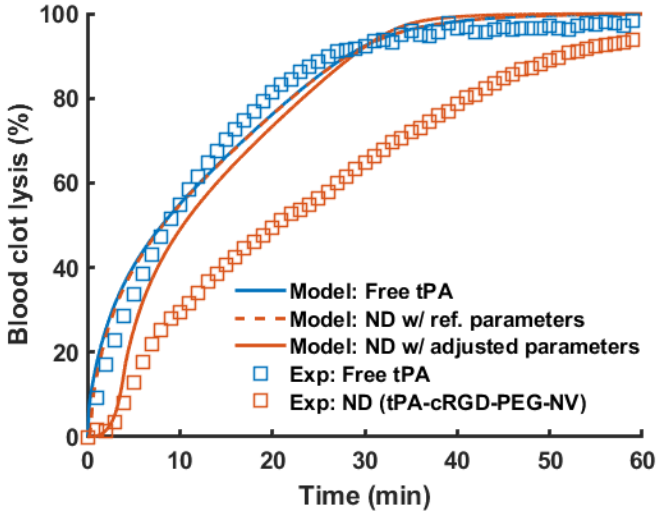

Figure S9. The extent of clot lysis in the halo human blood clot model obtained from the computational model (curves) and experiments (square symbols) with free tPA (blue) and the developed ND (orange). Two sets of model parameters for the ND are used: the reference set (dashed orange curve, $k_{a,ND}$ = 2.622×10^{-2} μM^{-1}·s^{-1}, $k_{d,ND}$ = 7.516×10^{-3} s^{-1} and k_{rel} = 0.1098 s^{-1}) and adjusted set (solid orange curve, $k_{a,ND}$ = 2.622×10^{-4} μM^{-1}·s^{-1}, $k_{d,ND}$ = 7.516×10^{-5} s^{-1} and k_{rel} = 0.01098 s^{-1}).

5.2. Additional simulation results for the static thrombolysis experiments

In order to provide more information on the behaviors of fibrinolytic proteins predicted by the computational model for the Halo human blood clot lysis experiments, temporal concentration profiles for all the species were examined. As shown in Figure S10 (for free tPA) and Figure S11 (for the ND), the main difference between the two simulated scenarios was the profile of C_{tPA}. tPA was rapidly consumed when free tPA was introduced, as can be seen in Figure S10. However, for the targeted thrombolytic system, C_{tPA} gradually increases over an hour while C_{ND} was consumed following triggered release, shown in Figure S11. This resulted in a difference in the profile of n_{PLS}, which directly affects the rate of fibrinolysis. However, the tPA concentration used in the experiment was excessively high compared to the typical therapeutic level. This led to the complete conversion of available PLG into PLS, as evidenced by C_{PLG} and n_{PLG} in both scenarios. Therefore, it is considered reasonable that complete thrombolysis was achieved within the time duration with free tPA and the ND as shown in Figure S9.

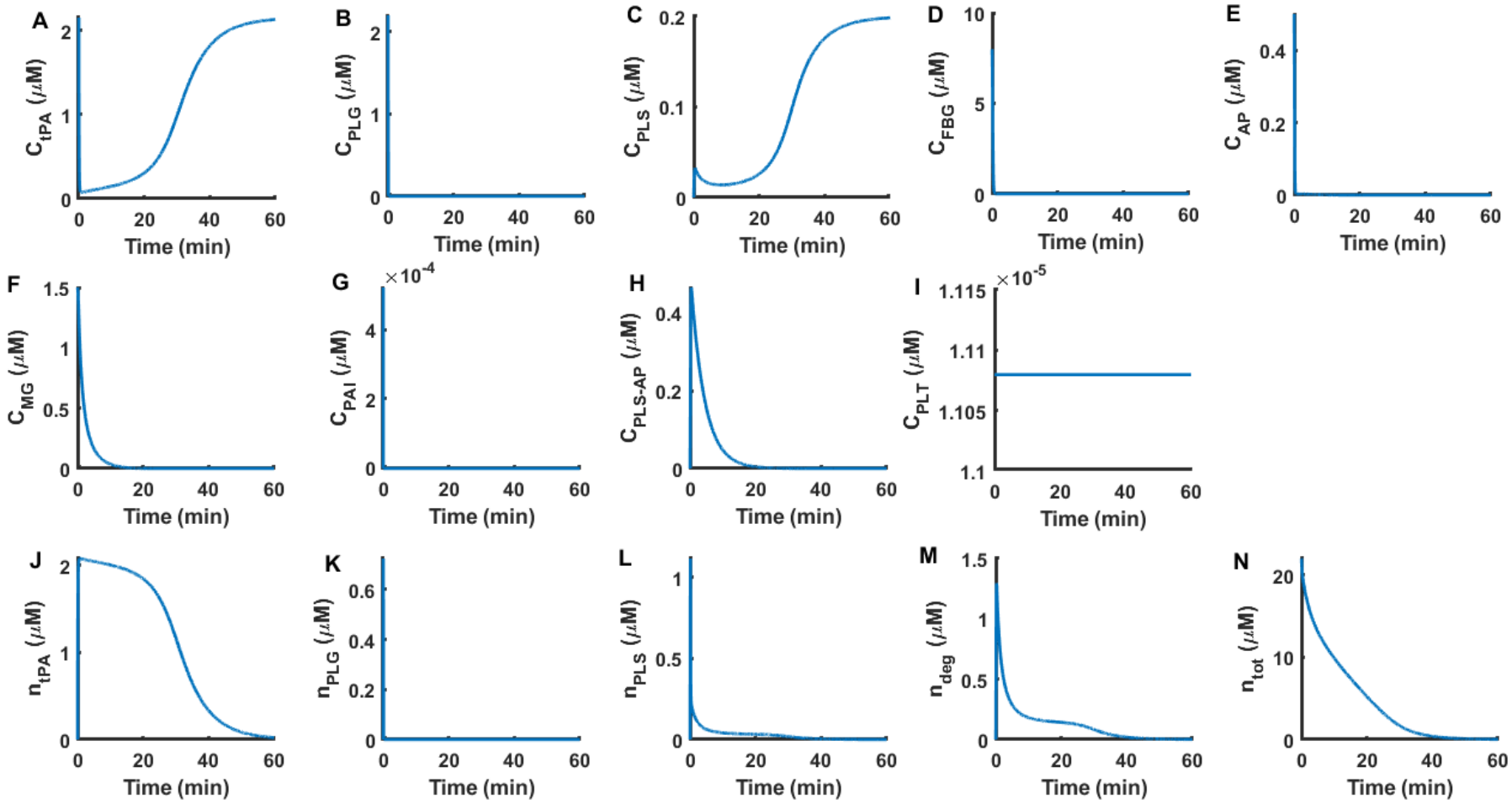

Figure S10. Temporal concentrations of all the species included in the model for the halo human blood clot lysis experiment with free tPA.

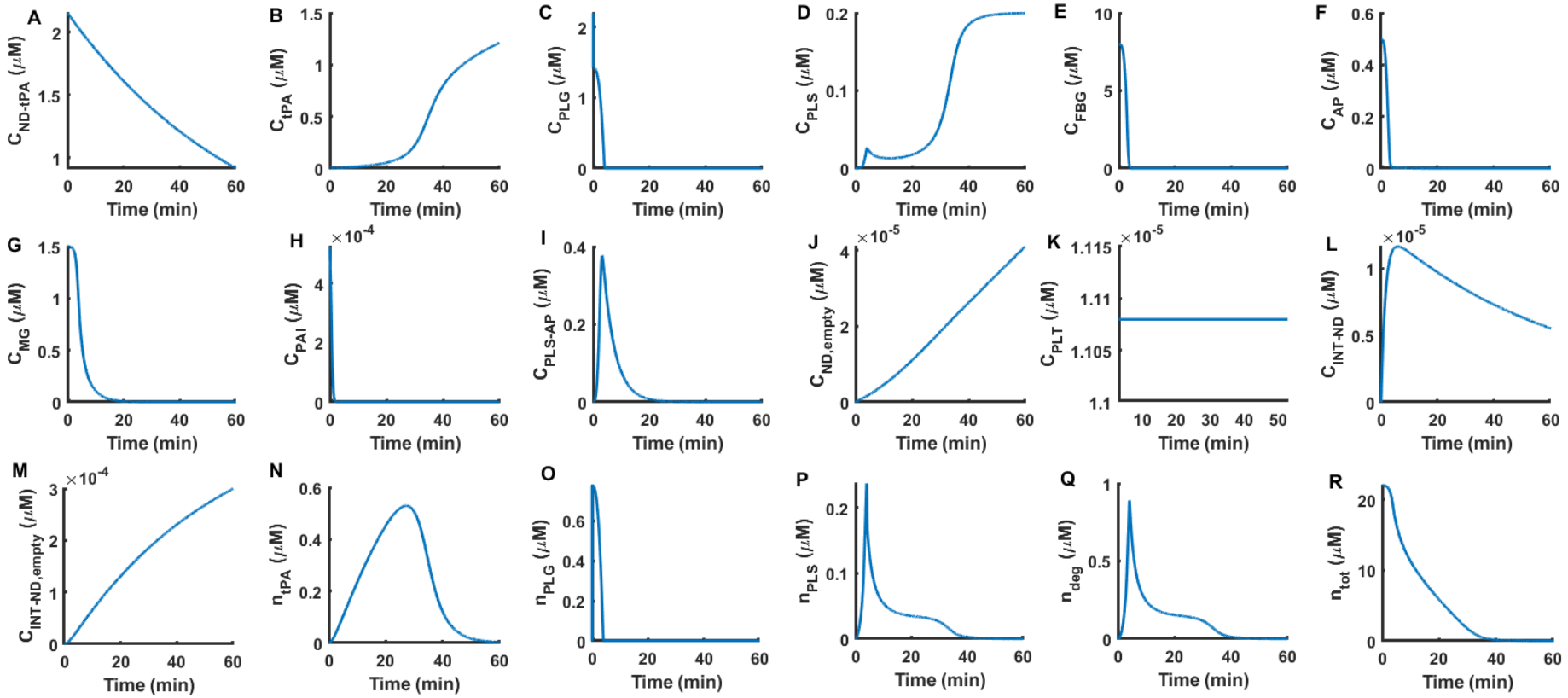

Figure S11. Temporal concentrations of all the species considered in the model for the Halo human blood clot lysis with the ND (tPA-cRCD-PEG-NV) with the adjusted parameter set ($k_{a,ND}$ = 2.622×10^{-4} μM^{-1} s^{-1}, $k_{d,NP}$ = 7.516×10^{-5} s^{-1} and k_{rel} = 0.01098 s^{-1}). $C_{ND\text{-}tPA}$ is the concentration of tPA encapsulated in the ND.

5.2. Additional simulation results for thrombolysis under flow conditions

In addition to the results presented in the manuscript, herein we include results for all the simulated scenarios under flow conditions. Figures S12 to S17 present variations in thrombus volume, averaged thrombus resistance, averaged volume fraction, extent of thrombolysis, and concentrations of key fibrinolytic proteins for 6 cases. There was a small reduction in the volume fraction of activated platelets within the thrombus. In the current model, the mobility of activated platelets in a thrombus was assumed to be either unity (free) when the critical extent of lysis was reached, or zero (trapped) as described in Eqs (S36) and (S37). As such, it did not fully capture the temporal release of platelets as the thrombus degraded. This can be improved by introducing an appropriate mobility function in the future.

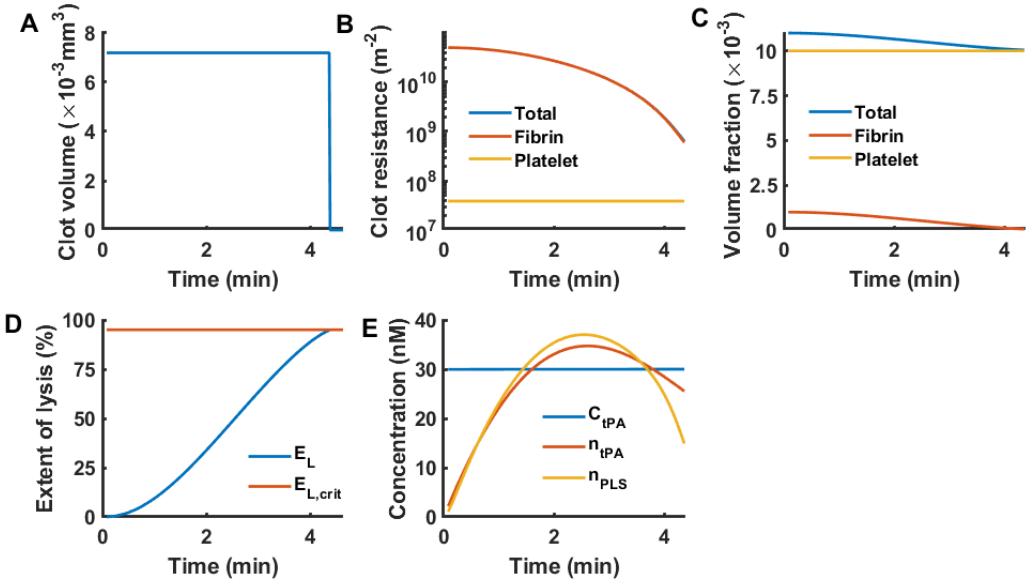

Figure S12. Simulation results for a small coarse thrombus treated with free tPA. The blue and orange curves in B are overlapped due to their negligible difference.

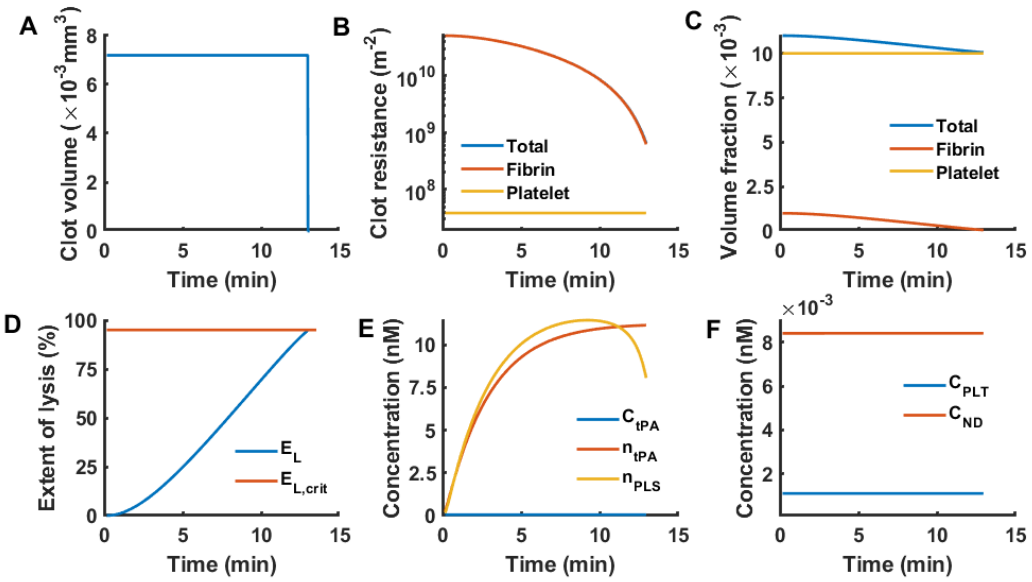

Figure S13. Simulation results for a small coarse thrombus treated with ND. The blue and orange curves in B are overlapped due to their negligible difference.

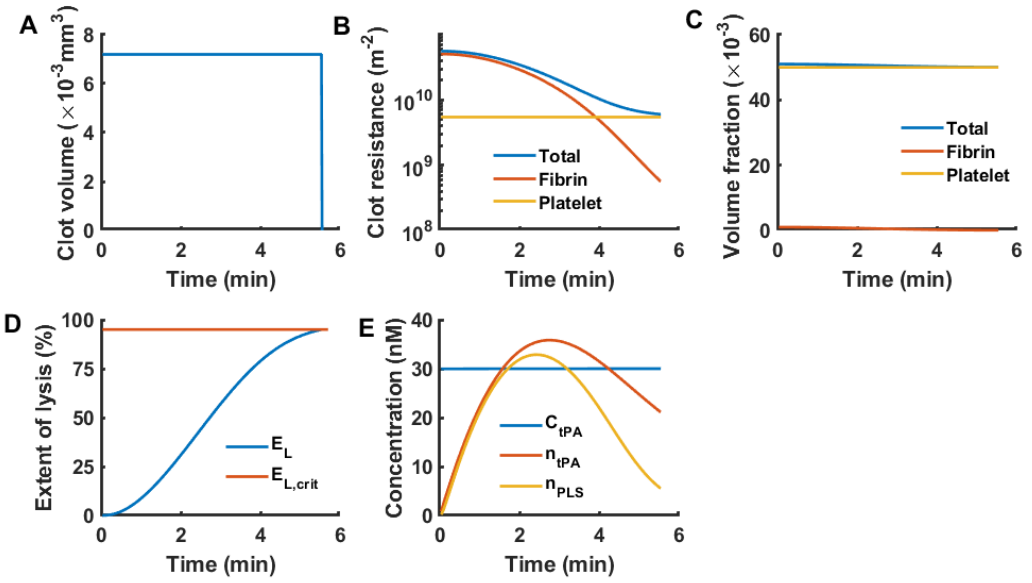

Figure S14. Simulation results for a small dense (platelet-rich) thrombus treated with free tPA.

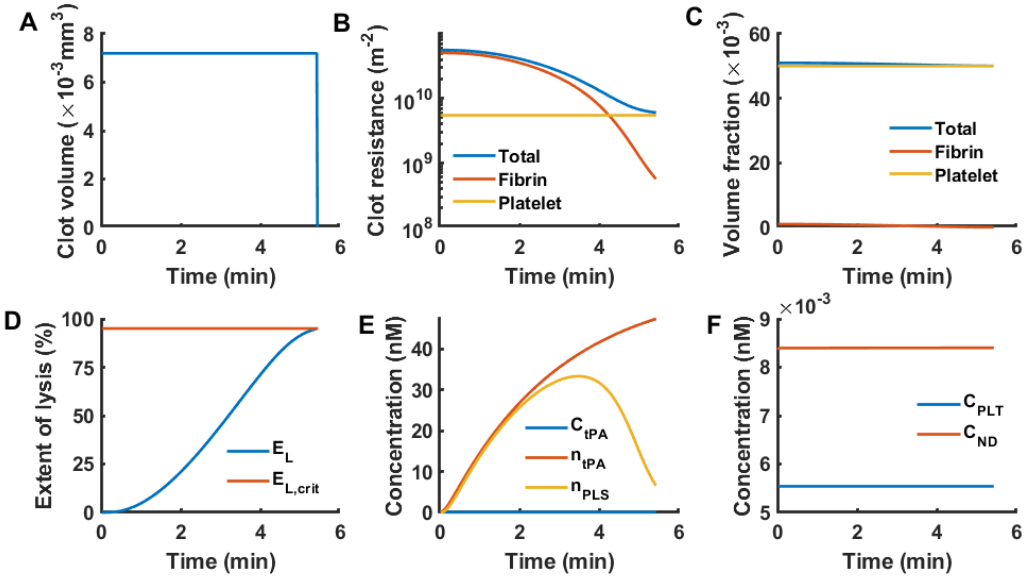

Figure S15. Simulation results for a small dense (platelet-rich) thrombus treated with ND.

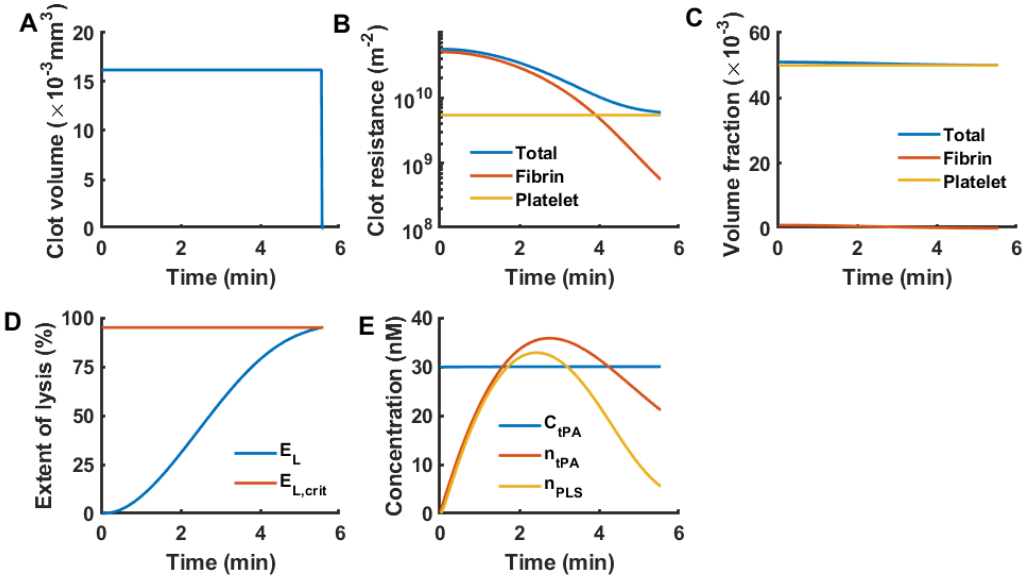

Figure S16. Simulation results for a large dense (platelet-rich) thrombus treated with free tPA.

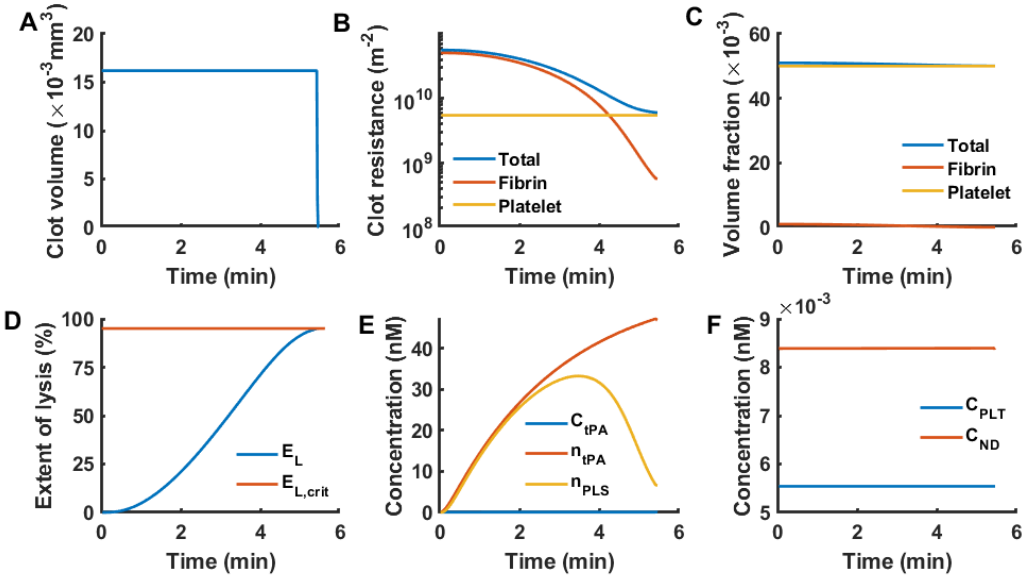

Figure S17. Simulation results for a large dense (platelet-rich) thrombus treated with ND.

6. Supplementary movies

Video S1. Real-time video of human blood clot lysis by cRGD-PEG-NV in the microfluidic system

Video S2. Real-time video of human blood clot lysis by tPA-PEG-NV in the microfluidic system

Video S3. Real-time video of human blood clot lysis by tPA-cRGD-PEG-NV in the microfluidic system

Video S4. Real-time video of human blood clot lysis by free tPA in the microfluidic system

Video S5. Animation of blood clot lysis produced by our computational model for tPA-cRGD-PEG-NV

Video S6. Animation of blood clot lysis produced by our computational model for free tPA